ASTRONOMY & ASTROPHYSICS
SUPPLEMENT SERIES

Astron. Astrophys. Suppl. Ser. **137**, 185–202 (1999)

3D mapping of optical turbulence using an atmospheric numerical model

I. A useful tool for the ground-based astronomy

E. Masciadri[1], **J. Vernin**[1], **and P. Bougeault**[2]

[1] U.M.R. 6525 Astrophysique, Université de Nice-Sophia Antipolis, Centre National de la Recherche Scientifique, Parc Valrose, 06108 Nice Cedex 2, France
[2] Centre National de Recherches Météorologiques Météo France, 42 Av. G. Coriolis, 31057 Toulouse, France

Received June 4, 1998; accepted February 4, 1999

Abstract. These last years have seen the development of many devices to measure and monitor some atmospheric parameters characterizing the image degradation at the telescope focus. Many uncertainties about the possibility to forecast such parameters are real although this skill is fundamental for site testing, flexible scheduling and optimization of the performance of both interferometry and adaptive optics. We present our atmospheric numerical model, conceived to provide 3D maps of the classic meteorological parameters P, T and $\boldsymbol{V}$, and also 3D maps of the C_N^2 optical turbulent profiles. Knowing the wind $\boldsymbol{V}$ and the C_N^2 profiles, the following integrated parameters are coded: seeing ε, coherence wavefront time τ_{AO}, isoplanatic angle θ_{AO}, scintillation rate σ_I^2 and spatial coherence outer scale $\mathcal{L}_0$.

The ability of the model to produce a 3D map of optical turbulence in the vicinity of a telescope and the effects of horizontal grid size are discussed. We demonstrate, for the same night, the global coherence of the different simulation outputs. Here we consider the use that this model could have in ground-based astronomy and we describe how it could be used to give a real *forecast* of the optical turbulence.

Key words: atmospheric effects, turbulence, site testing

1. Introduction

One of the most important problems for the ground-based astronomy is the limiting resolution of the image imposed by the atmospheric turbulence in addition to the limit imposed by the optical instrument. The large diameter of new telescopes increases the light collected by the instrument but it cannot help to get a better spatial resolution in the image. The atmospheric turbulence modifies in a stochastic way the amplitude and the phase of the incoming wavefront and the images appear degraded. Different parameters are used to characterize the turbulence intensity in the atmosphere: Fried's parameter r_0, the seeing ε, the C_N^2 profiles, the spatial coherence outer scale $\mathcal{L}_0$, the isoplanatic angles θ_{AO}, the scintillation rate ${\sigma_I}^2$, the speckle boiling time τ_s and the wavefront coherence time τ_{AO}. Each of these parameters has a relevance for particular astronomical applications. The outer scale $\mathcal{L}_0$, for example, is fundamental for stellar interferometry and, in general, for the large-ground-base interferometry as soon as the baseline is of the order or larger than $\mathcal{L}_0$. It is known that the optical bandwidth $\Delta\lambda$ is limited by the wavefront coherence. If the base line L is less than $\mathcal{L}_0$ then

$$\Delta\lambda = 0.45\lambda \left(\frac{r_0}{L}\right)^{5/6} \quad (1)$$

but, if $L > \mathcal{L}_0$ then

$$\Delta\lambda = 0.45\lambda \left(\frac{r_0}{\mathcal{L}_0}\right)^{5/6}. \quad (2)$$

In this case, the minimum optical bandwidth depends on $\mathcal{L}_0$.

The isoplanatic angle θ_{AO} is a critical parameter for adaptive optics and laser guide star technique. We remember that, for example, the number of artificial stars necessary for a complete sky covering is proportional to the inverse of the square of the isoplanatic angle (Chester et al. 1990) $N_G \sim 1/\theta^2$. The coherence wavefront time τ_{AO} is particularly interesting because it gives information about the so-called Greenwood frequency $f_G = 0.135/\tau_{AO}$ which is often used in specification of adaptive optics control systems (Beckers 1993).

Send offprint requests to: E. Masciadri

At present, there are many reliable techniques (direct and indirect) and instruments used to measure these parameters. We recall the DIMM (Sarazin & Roddier 1981) for the seeing, the SCIDAR (Vernin & Azouit 1983a,b) (optical measurements) and the instrumented balloons (in situ measurements) for the C_N^2 profiles, the GSM (Martin et al. 1994) for the spatial coherence outer scale. These instruments are expensive, need a lot of man-power, provide the relevant parameter for only one site and one line of sight and have no predictive capability. In order to overcome these restrictions, following previous attempts, we propose to use a meteorological model coupled with a set of equations which links optical turbulence and the air flow. In the past, some attempts have been made in the study of seeing forecasting but none of the techniques previously tried could resolve the issue by itself. The reasons of this failure is the following. The seeing value is correlated to meteorological parameters like the temperature, wind intensity and direction and to geographic parameters like the orography. The problem is that the spatial and temporal fluctuation scales of the seeing are much smaller than the highest resolution attained by typical large scale (synoptic) meteorological forecasts. We prefer, so, a medium-range scale model. We give a brief summary of some of the interesting applications that this technique could have in the astronomical context.

Besides an accurate climatology, and a nowcasting technic (Murtagh & Sarazin 1983), such a numerical model could be a useful tool for site testing. In spite of the recent excellent results obtained by space telescopes, ground-based astronomy is today still competitive in many fields. Finding the best place to install large modern telescopes ($\geq$ 8 m) is fundamental to attain the maximum efficiency.

Moreover, the scientific potential of the new generation telescopes is measured not only by the performance of the instruments placed at the focus of the telescope but by their proper use. The optimization of the "observing time programs" (flexible scheduling) is mandatory to make a telescope competitive (Di Serego 1996; Di Serego 1997; Sarazin 1997; Masciadri et al. 1997). If very good seeing is predicted in the next few hours, optimized management of an observatory might decide to use high angular resolution instrument instead of a photometric one. However this is not an easy goal: seeing measurements obtained during the past campaigns (Munoz-Tuñón et al. 1997; Sarazin 1997; Racine 1996), show a short temporal stability (seeing characteristic time) of the order of $20 - 30$ min. We intend to study whether an optimized numerical model could help in nightly programming the telescope observing time.

Finally, with a numerical technique we could obtain a global optical turbulence characterization. For a given time t_0, 3-D maps (x, y, z) of all the parameters characterizing the optical turbulence in a region around the telescope could be forecast and we could estimate integrated values along different lines of sight. Hence, it is be better to talk about an "Optical Turbulence Forecast" instead of a simple "Seeing Forecast".

What is the state of the art of the seeing forecast for astronomical applications? We summarize, here, some of the most significant approaches provided by the literature.

Statistical technique
A statistical multiple regression (nearest-neighbor regression) was applied to Paranal and La Silla sites (Murtagh 1993). This technique is not a true prediction but rather a "nowcasting". It tries to relate seeing measurements to meteorological and environmental conditions at the same time or in the near past.

Dynamical recurrent neural networks technique
The neural network is a non linear approach to data series treatment. Its advantage, when compared to a statistical one, is that it has a sort of inside memory that is the possibility to re-assimilate not only the recent data but also the data of the past. Some authors (Aussem et al. 1994) tried to apply it to the astro-climatic forecasting but, to our opinion, they did not obtain particularly encouraging results.

Physical model technique
In the last decade, some authors (Coulman et al. 1988) proposed a new approach based on the measurements of the vertical gradient of the temperature. Assuming a universal behavior of the outer scale of turbulence they deduced the vertical profile of the optical turbulence C_N^2.

A different approach was tested by Van Zandt (Van Zandt et al. 1978, 1981). In the absence of any estimation of the geophysical outer scale L_0, the authors developed a stochastic model based on a statistical treatment of the atmospheric vertical "fine structure". This model was first used for astronomical purpose at the CFH telescope in Hawaii (Bely 1983) and it led to a poor correlation due to the impossibility of discriminating between boundary layer, dome and tracking seeing.

More recently, following the suggestions of a pioneering article (Coulman & Gillingham 1986) which proposed of numerical modeling, the authors (Bougeault et al. 1995) implemented the hydrostatic numerical model PERIDOT to forecast the seeing above a French site (Mt. Lachens). The model had a 3 km $\times$ 3 km resolution and it was supported by the French radiosounding network, enabling good initialization of the model. It gave satisfactory results but with some limitations:

1. The simulations give a lot of information but many discrepancies are still observed.
2. The poor spatial correlation is probably due to a lack of resolution of the model.
3. The model can discriminate between good and bad seeing but only in a qualitative way.
4. No comparison of measured and simulated vertical C_N^2 profiles were realized, only integrated values of seeing ε were compared.

The model has not been applied yet to a high quality site. The best sites in the world have a mean seeing value of $[0.5 - 1]$ arcsec with a very small fluctuation range of about $[0.4 - 1.5]$ arcsec. Can numerical models forecast such low values? Can they forecast seeing with such a high precision as to discriminate between values in such a range?

In our opinion, the above mentioned limitations are due to the fact that the meteorological model was hydrostatic and thus it could make a significant error on the small scale component of the vertical velocity. It is true that in most cases, over flat terrain, one can assume a pure horizontal flow (hydrostatic hypothesis). Good observatories are generally installed on the top of high mountains and local effects are expected since the horizontal flux hits steep slopes. At observatory altitudes, ranging mainly between 2000 and 4000 meters, one can find strong winds that induce lee waves close to the summit and gravity waves can be encountered at higher altitudes, from say 5 to 15 km. It is known (Coulman et al. 1995; Tennekes & Lumley 1972; Tatarski 1961; Meteorological Monographs 1990) that optical turbulence is triggered by phenomena such as lee waves, gravity waves, jet stream or wind shear. Hence, it seems mandatory to us to discard the hydrostatic hypothesis and use the full non hydrostatic equations in the predicting model. Furthermore, many authors already noticed that most of the optical turbulence is concentrated in the boundary layer (the first kilometer) which is well taken into account by the use of both non-hydrostatic flow and fine horizontal grid size.

2. Feasibility study

The results reported in this article were produced by a collaboration between the DA (Astrophysical Departement of Nice University) and the CNRM (Centre National des Recherches Meteorologiques) to provide ESO (European Southern Observatory) with an assessment of the potential and limitations of seeing prediction in the context of a flexible operation mode for the VLTI. In order to verify the technical feasibility, we compared the MESO-NH model (mesoscale, non-hydrostatic) simulations with the optical measurements obtained during the PARSCA93 campaign at Paranal (Fuchs & Vernin 1994) by the team of Nice University of J. Vernin and by M. Sarazin of ESO. During this campaign both the seeing and C_N^2 profiles were assessed. To our knowledge, it is the first time that such a detailed comparison has been attempted. A forthcoming article will be devoted to a complete statistical comparison of the PARSCA93 campaign and our simulations. In this paper we intend to present a detailed description of the Meso-Nh model and its performance related to the astronomical application of seeing forecasting. The astronomical code has now been adapted to simulate all the principal atmospheric parameters that are necessary for the exploitation of a telescope and the selection of different observing modes: Direct Imaging, Spectroscopy and Interferometry (Site selecting workgroup 1990).

In order to better study the model performances we used a simple model configuration. We first initialize the numerical model with orographically unperturbed meteorological data provided by either Meteorological Station radiosounding (Antofagasta station in our case) or ECMWF (European Center for Medium Weather Forecast) data analysis computed in the nearest grid point to the meteorological station. Both the station and the analysis grid point are located north-west of the Paranal mountain. Knowing that the prevailing wind blows in a NW-SE direction, we can reasonably consider that the atmosphere above the Antofagasta station is unperturbed by orography. We start the numerical simulations, at the initial instant t_0, with a uniform distribution of meteorological parameters inside each horizontal plane. Then the model simulates the effects of the adjustment to orographic forcing in a realistic way. After a certain lapse of time, the system converges to a stable solution or it oscillates around an equilibrium condition. We validate the model results by comparing with optical measurements (realized with a SCIDAR and DIMM techniques) related to a precise night, hour and for a selected time interval.

3. Meso-Nh fundamental equations

3.1. General characteristics

The Meso-Nh Atmospheric Simulation System (Lafore et al. 1998) can simulate the time evolution of the atmospheric three dimensional motions ranging from the large meso-alpha scale (100 km) down to the typical microscale of the Large Eddy Simulation (LES) models (50 m). It can forecast several meteorological variables on its 3D computation grid: the three components of the wind, the temperature, the moisture, the pressure and the turbulence kinetic energy. An optical turbulence scheme has been added later and is sketched in Sect. 3.3 (seeing ε, C_N^2 profiles, isoplanetic angle θ_{AO}, scintillation rate σ_I^2, coherence wavefront time τ_{AO} and spatial coherence outer scale $\mathcal{L}_0$). Meso-Nh is a non-hydrostatic numerical model (Lafore et al. 1998) based on the anelastic approximation. The principal characteristic of this approximation is that all acoustic waves are filtered but nevertheless, the model can represent accurately the gravity waves that enhance the shear production of turbulence. The lee waves occurring downstream of the mountain ranges and resulting in flow deceleration are particularly well simulated by this model. These waves can perturb the flow and increase the level of the turbulence activity. Using a high model resolution, we need a non-hydrostatic model to resolve the orographic effects in the turbulence developement and obtain

a more accurate estimation of the turbulent kinetic energy because such a model describes this physical phenomenon.

The input data required by the model are:

- a numerical terrain model with high spatial resolution;
- the fields of atmospheric pressure, temperature, humidity and wind known at an initial time t_0. One can use either analyses provided by Meteorologic Centers or radiosoundings provided by Meteorological Stations.

3.2. Dynamical turbulence parameterization

The basic equations of the model that are used to compute the time evolution of the physical system are the conservation of momentum (equations of motion), the first law of thermodynamics combined with equation of state and the equations of dry-air-mass and moisture conservation. The turbulence is among the physical processes that occur at scales too small to be resolved by the model and so it must be parameterized. Although the model offers a choice of 3D turbulent schemes, we used a 1D mode which takes into account only the vertical turbulent fluxes. The method used to describe the turbulence production is detailed in previous papers (Bougeault et al. 1995, 1989). It relies on the turbulence kinetic energy equation which takes the following form in Meso-Nh (Cuxart et al. 1995):

$$\frac{De}{Dt} = -\overline{w'u'}\frac{\partial U}{\partial z} - \overline{w'v'}\frac{\partial V}{\partial z}$$

$$+\frac{1}{\rho}\frac{\partial}{\partial z}(0.2\rho L\sqrt{e}\frac{\partial e}{\partial z}) - 0.7\frac{e^{\frac{3}{2}}}{L} + \beta\overline{w'\theta_v{}'}$$

where the first and second term on the right hand side represent the shear production, the third term the diffusion and the fourth term the dissipation. The last term is the buoyancy term: $w^{'}$ is the vertical wind fluctuation, $\theta_v^{'}$ the virtual potential temperature fluctuation and $\beta = g/\theta_v$ (g is the gravity acceleration). The vertical fluxes of wind and temperature are parameterized following the eddy diffusivity approach:

$$\overline{w'\theta'_v} = -K\frac{\partial\overline{\theta_v}}{\partial z}. \tag{3}$$

The physical parameterizations are somewhat different from those of the previous hydrostatic model Peridot (Bougeault 1995) developed at the CNRM in Toulouse (Fr). In the Peridot model, the eddy diffusivity is given by:

$$K(x,y,z,t) = 0.4L(x,y,z,t)\sqrt{e(x,y,z,t)} \tag{4}$$

where L is a mixing length. In Meso-Nh the eddy diffusivity is a function given by:

$$K(x,y,z,t) = 0.16L(x,y,z,t)\sqrt{e(x,y,z,t)}\phi_3(x,y,z,t) \tag{5}$$

where $\phi_3(x,y,z,t)$ is an inverse turbulent Prandtl number.

- L is the so called Bougeault-Lacarrere (BL89) (Bougeault 1989) mixing length defined as follows: at any level z in the atmosphere a parcel of air of given turbulence kinetic energy $e(z)$, can move upwards ($l_{\rm up}$) and downwards ($l_{\rm down}$) before being stopped by buoyancy forces. These distances are defined by:

$$\int_z^{z+l_{\rm up}} \frac{g}{\theta_v}\left(\theta_v(z) - \theta_v\left(z^{'}\right)\right)\mathrm{d}z^{'} = e(z) \tag{6}$$

and

$$\int_{z-l_{\rm down}}^{z} \frac{g}{\theta_v}\left(\theta_v\left(z^{'}\right) - \theta_v(z)\right)\mathrm{d}z^{'} = e(z) \tag{7}$$

L is defined as:

$$L = (l_{\rm up}l_{\rm down})^{1/2} \tag{8}$$

- ϕ_3 is a dimensionless function Redelsper & Sommeria (1981). It characterizes the thermal and dynamic stability of the atmosphere and takes into account the spatial variations of temperature, humidity and velocity components. This is an element that permits a parameterization of the model at different scales of motion. Its 3D analytical expression is given in Redelsperger & Sommeria (1981). It is a complex equation linked to the "Redelsperger numbers" (dimensionless numbers characterizing the thermal and dynamic stability). In a dry 1D option we have a simpler analytical expression:

$$\phi_3(x,y,z,t) = \frac{1}{1 + C_1\frac{L^2}{e}\frac{g}{\theta_v}\frac{\partial\theta_v}{\partial z}} \tag{9}$$

where $C_1 = 0.139$, and L is the above defined mixing length.

L^2/e behaves in a different ways in stable and unstable layers. In a very stable layer the mixing length is nearly equivalent to the Deardoff length

$$L = \sqrt{\frac{2e}{\frac{g}{\theta_v}\frac{\partial\theta_v}{\partial z}}}. \tag{10}$$

Replacing Eq. (10) in Eq. (9) leads to $\phi_3 = 0.78$. In a very unstable layer ϕ_3 takes larger values and an upper bound is set as $\phi_3 = 2.2$, based on theoretical and experimental results.

Finally, if we substitute Eqs. (5) in (3), we obtain the microscopic quantities related to the macroscopic variables L, e and ϕ_3.

$$\overline{w'\theta'_v} = -0.16L\sqrt{e}\phi_3\frac{\partial\overline{\theta_v}}{\partial z}. \tag{11}$$

3.3. Optical turbulence parameterization

The Meso-Nh model has been adapted to simulate the optical atmospheric turbulence which is estimated by measuring the structure constant of the temperature fluctuations (Wyngaard et al. 1971; André et al. 1978; Coulman et al. 1986):

$$C_{\rm T}^2 = 1.6\varepsilon_\theta \varepsilon^{-1/3} \tag{12}$$

ε_θ is the rate of temperature variance destruction by viscous processes and ε is the rate of energy dissipation related to the turbulence characteristic length L and the energy e by the Kolmogorov law

$$\varepsilon = 0.7\frac{e^{3/2}}{L}\cdot \tag{13}$$

Equation (12) assumes that θ is a passive additive constituent. This is not true in general since buoyancy forces are associated with temperature inhomogeneities and those buoyancy forces are taken into account in other aspects of our computation by the ϕ term. This theory is based on the analogy between the velocity fluctuations in a turbulent flow and the concentration fluctuations of a conservative passive additive θ in a turbulent flow. It is based on a law that links the microscopic and the macroscopic physical parameters. The prognostic equation of the potential temperature variance $\overline{\theta'^2}$ in the turbulent energy budget is (André et al. 1978):

$$\frac{\partial\overline{\theta'^2}}{\partial t} = -\frac{\partial\overline{w'\theta'^2}}{\partial z} - 2\overline{w'\theta'}\frac{\partial\overline{\theta}}{\partial z} - \varepsilon_\theta - \varepsilon_{\rm R} \tag{14}$$

where ε_θ is the molecular dissipation and $\varepsilon_{\rm R}$ the radiative dissipation. Assuming that we can neglect the contributions from the triple correlations $\overline{w'\theta'^2}$ and the radiative dissipation we have

$$\frac{\partial\overline{\theta^{2\prime}}}{\partial t} = -2\overline{w'\theta'}\frac{\partial\overline{\theta}}{\partial z} - \varepsilon_\theta. \tag{15}$$

The steady state balance equation for the rate of destruction of the variance leads to:

$$\varepsilon_\theta = -2\overline{w'\theta'}\frac{\partial\overline{\theta}}{\partial z}\cdot \tag{16}$$

If we substitute (16) and (13) into (12) using Eq. (11) presented in the last paragraph we obtain $C_{\rm T}^2$ expressed as a function of macroscopic variables only

$$C_{\rm T}^2 = 0.58\phi_3 L^{4/3}\left(\frac{\partial\overline{\theta}}{\partial z}\right)^2. \tag{17}$$

Finally, the structure constant of the refraction index is obtained using the Gladstone's law:

$$C_{\rm N}^2 = \left(\frac{80\ 10^{-6}P}{T^2}\right)^2 C_{\rm T}^2. \tag{18}$$

3.4. Optical turbulence code for Astronomy

Today we need to measure seeing and other parameters such as the coherence wavefront time ($\tau_{\rm AO}$), the isoplanatic angle ($\theta_{\rm AO}$) and the spatial coherence outer scale ($\mathcal{L}_0$). All these parameters are related to the refractive index fluctuations which appear inside the atmospheric turbulent layers and to the wind velocity profile. We summarize, in the following, the parameters which have been coded in the model. All the following parameters are referred to the zenith direction. Starting from the Fried parameter r_0 given by:

$$r_0 = \left[0.423\left(\frac{2\pi}{\lambda}\right)^2 \int_0^\infty C_{\rm N}^2(h)\,{\rm d}h\right]^{-3/5} \tag{19}$$

the seeing ε, defined as the width at the half height of a star image at the focus of a large diameter telescope was expressed as follows (Roddier 1981):

$$\varepsilon = 0.98\frac{\lambda}{r_0} \tag{20}$$

where λ is the optical wavelength. As others authors we choose $\lambda = 0.5\ 10^{-6}$ m for this study.

The isoplanatic angle $\theta_{\rm AO}$ (Roddier et al. 1982; Fried 1979) defined as the maximum angular separation of two stellar objects producing similar wavefronts at the telescope entrance pupil, has the following analytical expression:

$$\theta_{\rm AO} = 0.31\frac{r_0}{h_{\rm AO}}. \tag{21}$$

Knowing that the seeing layer $h_{\rm AO}$ is a sort of average distance weighted by a 5/3 power law

$$h_{\rm AO} = \left[\frac{\int_0^\infty h^{5/3}C_{\rm N}^2(h)\,{\rm d}h}{\int_0^\infty C_{\rm N}^2(h)\,{\rm d}h}\right]^{3/5} \tag{22}$$

we obtain

$$\theta_{\rm AO} = 0.057\cdot\lambda^{6/5}\left(\int_0^\infty h^{5/3}C_{\rm N}^2(h)\,{\rm d}h\right)^{-3/5}. \tag{23}$$

The scintillation rate (Roddier 1981) was expressed as follows

$$\sigma_{\rm I}^2 = 19.12\lambda^{-7/6}\int_0^\infty h^{5/6}C_{\rm N}^2(h)\,.{\rm d}h \tag{24}$$

The coherence wavefront time $\tau_{\rm AO}$ (Roddier et al. 1982) is:

$$\tau_{\rm AO} = 0.31\frac{r_0}{\upsilon_{\rm AO}} \tag{25}$$

where

$$\upsilon_{\rm AO} = \left[\frac{\int_0^\infty |\boldsymbol{V}(h)|^{5/3}\,C_{\rm N}^2(h)\,{\rm d}h}{\int_0^\infty C_{\rm N}^2(h)\,{\rm d}h}\right]^{3/5} \tag{26}$$

and $\boldsymbol{V}$(h) is the horizontal wind velocity vector. Thus, $\tau_{\rm AO}$ can be expressed as:

$$\tau_{\rm AO} = 0.057 \cdot \lambda^{6/5} \left[\int_0^\infty |\boldsymbol{V}(h)|^{5/3} C_{\rm N}^2(h)\, {\rm d}h \right]^{-3/5}. \quad (27)$$

Finally, the spatial coherence outer scale (Borgnino 1990)

$$\mathcal{L}_0 = \left[\frac{\int_0^\infty L(h)^{-1/3} C_{\rm N}^2(h)\, {\rm d}h}{\int_0^\infty C_{\rm N}^2(h)\, {\rm d}h} \right]^{-3} \quad (28)$$

where L is the Bougeault-Lacarrere mixing length defined in Sect. 3.2.

4. Meso-Nh model initialization

4.1. Orographic model

The results presented in this paper have been obtained using a high resolution orographic model (500 m × 500 m) centered on Paranal mountain (70.40 W, 24.61 S). In Fig. 1 we display the 2D map of the orographic model related to the total available surface domain. It corresponds to a domain of 60 km × 60 km, that is a 120 × 120 grid point matrix. Two horizontal dashed lines mark the extension of a second orographic model related to a reduced portion, still preserving the general geographic structure of the region: a sea shore to the west, a sharp mountain chain along the Chilean coast, a broad mountainous region which includes the peak of Paranal and a few higher mountains to the east of Paranal. It corresponds to a domain of 60 km × 20 km sampled on 120 × 40 grid points, which was used for all the simulations presented in this paper.

4.2. Input data for the model initialization

The model initialization is critical for the numerical technics. After a simulation, the quality of the output and the input data are strictly correlated. We used, as input data, the ECMWF analysis taken at the (70.31 W, 23.62 S) grid point and the radiosounding from Antofagasta station (70.43 W, 23.43 S). The analysis are 3D fields at low spatial resolution produced by the meteorological centers for forecast needs. A more detailed analysis of the data that we used will be given in a further article. The numerical model is initialized with a vertical profile of P, q, T, U, V (pressure, humidity, temperature and wind) describing the meteorological situation of a given night, upstream with respect to the wind direction, from the geographical region analyzed. The forecast values of the hydrodynamic variables of the prognostic equations provided by the model are produced following a deterministic computation. One can expect that the higher the spatial vertical resolution of the different parameters (P, T, $\boldsymbol{V}$) the better the precision and sensitivity of the simulations will be. In general, the meteorological radiosoundings have a better vertical resolution than the analysis but they have a poorer temporal sampling (at the best, only two measurements are available each day). Moreover the station density is not uniformly distributed over the world.

4.3. Spatio-temporal x, y, z, t initialization

For all simulations presented in this paper, a computational time step $t_{\rm s} = 2.5$ s was found to be necessary to achieve stable simulations (Masciadri et al. 1997). We analyzed 60 × 20 km around the Paranal mountain with an horizontal resolution of 500 m. We used the following vertical resolution: 50 m for the first vertical mesh $\Delta z(1)$, a vertical stretching of 30% over the first 3 km that is

$$\frac{\Delta z(k+1)}{\Delta z(k)} = 1 + 30/100 \quad (29)$$

and a constant resolution of 600 m from 3 km to 20 km. The choice of the stretching for the lowest grid points was made to save computing time, preserving maximum resolution where the effects of orography are the most important and the development of turbulent eddies is the most efficient. The atmosphere is thus sampled on 40 levels with a vertical resolution ranging from 50 near the ground to 600 m at high altitude.

5. Meso-Nh outputs and performances

5.1. Simulation of the flow by the model

To generate optical turbulence it is necessary to have both a temperature gradient and a dynamic instability (Coulman et al. 1995). We analyze first the thermic and then the dynamic sources of turbulence related to the 16/5/93 night of the PARSCA93 campaign in order to give an explicit demonstration that the lee waves produced by the high mountain steps are correctly resolved by the model. The temporal evolution of the potential temperature over 4 hour simulation time is reported in Figs. 2a-c. High density isolines regions correspond to static stability and low density isolines are associated with static instability. The irregular isolines indicate the presence of gravity waves. The source of these waves is the steep chilean coast and the waves propagate in the interior region (quoted by two straight lines in Figs. 2a-c) of the atmosphere over Paranal mountain. This suggests that some optical turbulence over Paranal is generated far away over the chilean coast. Figure 3 shows a vertical section of the vertical wind fluctuations selected over 40 km along the east-west direction centered over Paranal mountain. The alternation of positive and negative values is a further proof of the presence of gravity waves. This particular structure of the

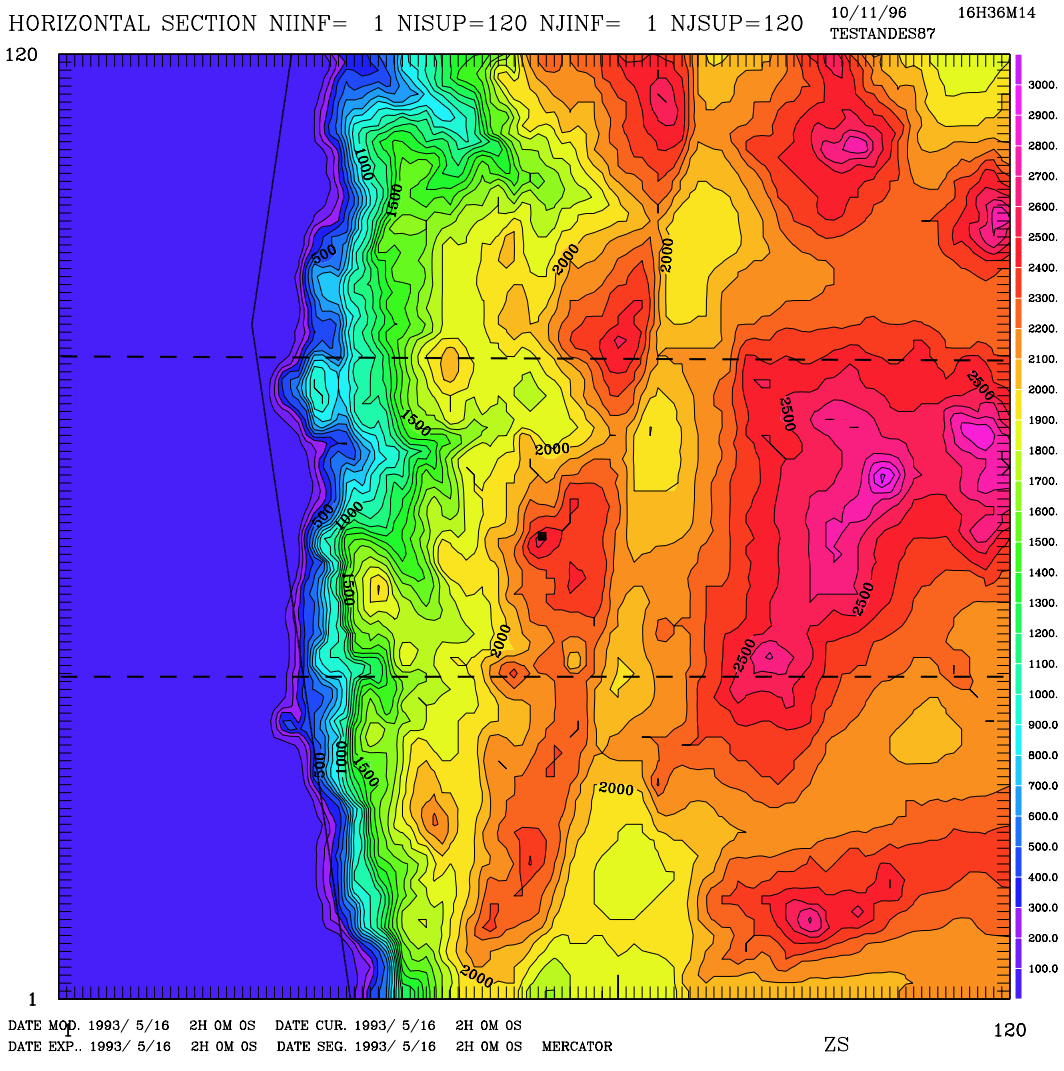

Fig. 1. Orographic model - 120 × 120 grid points equivalent to 60 km × 60 km - Horizontal resolution: 500 m × 500 m. The position of the Paranal mountain is marked by a black square. Dashed lines mark the domain used for the simulations presented in this article: 60 km × 20 km. *Colour figure on Web A&AS site*

isolines in the first 10 km attests the sensitivity of the model in this part of the atmosphere. In Fig. 4 we report profiles of the wind vertical fluctuations obtained after 30 minutes, 1 hour and 4 hours of simulation time. The vertical wave propagation is deduced from the temporal sequence of images. Values of the order of 1 m/s in the first 12 km suggest that the model is capable of representing this aspect of the atmospheric dynamics. Finally in Fig. 5 we show a vertical section of the turbulence kinetic energy produced by orographic effect not only at the ground but also at higher altitudes (8000 m). The mixing length, shown in Fig. 6, is strongly correlated to energy e.

5.2. Simulation time to achieve a steady - state

Particular attention must be paid to define the simulation time necessary to adapt the flow to the orography and to converge to a steady state (*spin-up* time). We should expect that the adaptation time will, in general, depend on the initial configuration. In general, starting a simulation in a near dynamic equilibrium state will produce a faster adaptation process. In order to estimate this time we modified the code to have access to the temporal seeing evolution sampled with 2.5 s. Figure 7 shows the simulated temporal seeing evolution over Paranal related to the best and the worst PARSCA93 campaign nights with respect to the mean value of the whole campaign. During the 25/5/93 night (the best one), after about 1 hour, the seeing is oscillating around its mean value (0.7 arcsec). On the contrary, during the 16/5/93 night (the worst one) the seeing seems stable and, suddenly, increases to up 1.5 arcsec after 9 000 and 14 000 s, with a more chaotic trend. On this night, the strong degradation of the seeing is associated with the appearance of a turbulent layer at 4 km as one can see on the C_N^2 profile Fig. 8. This turbulent layer is correlated to the gravity waves already

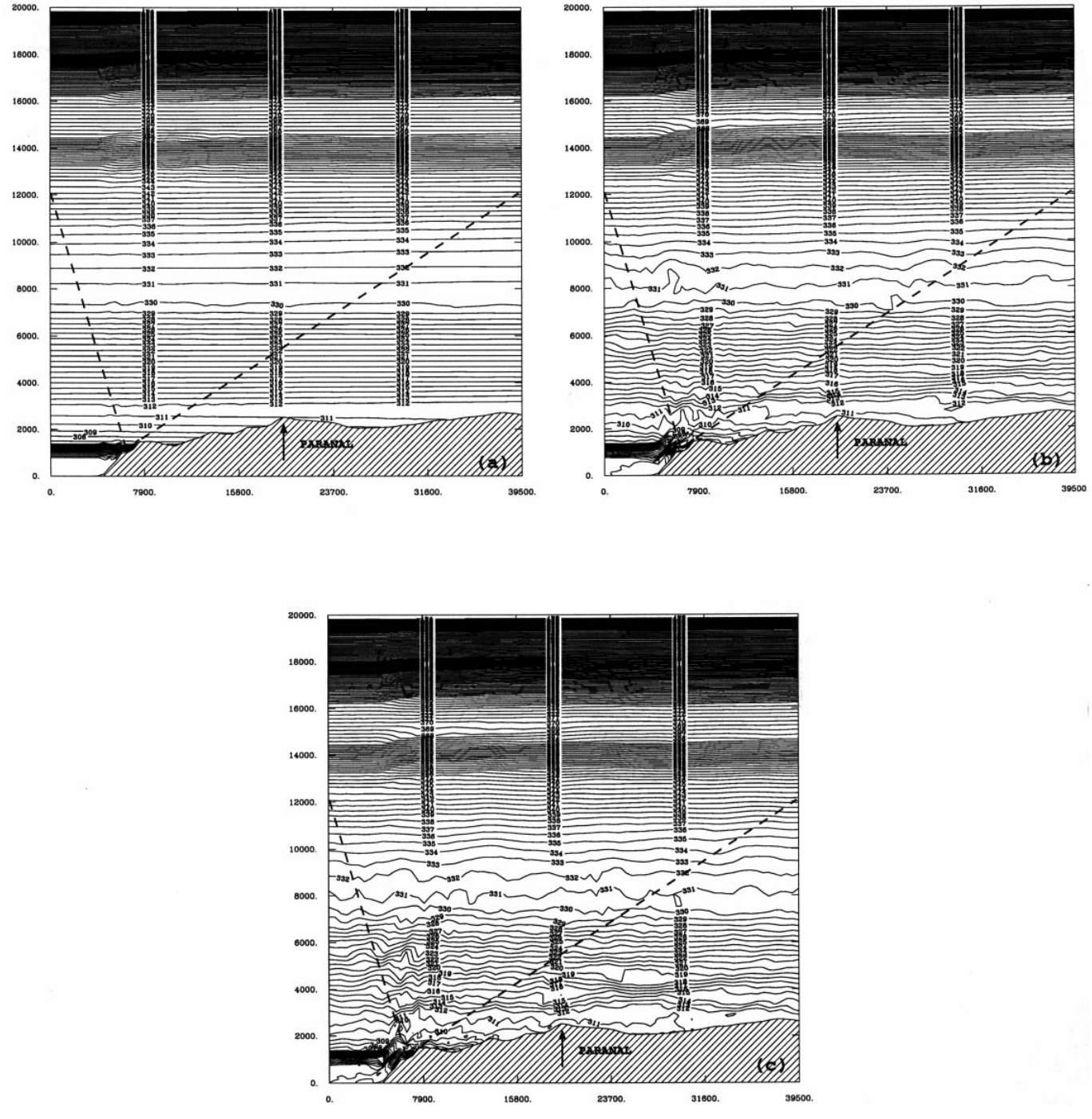

Fig. 2. Potential temperature east-west vertical sections across the Paranal mountain extended over 40 km with a resolution of 500 m. Meso-Nh outputs during the 16/5/93 night (PARSCA93 campaign) at different simulation times. After **a)** 0 hours **b)** 2 hour **c)** 4 hours

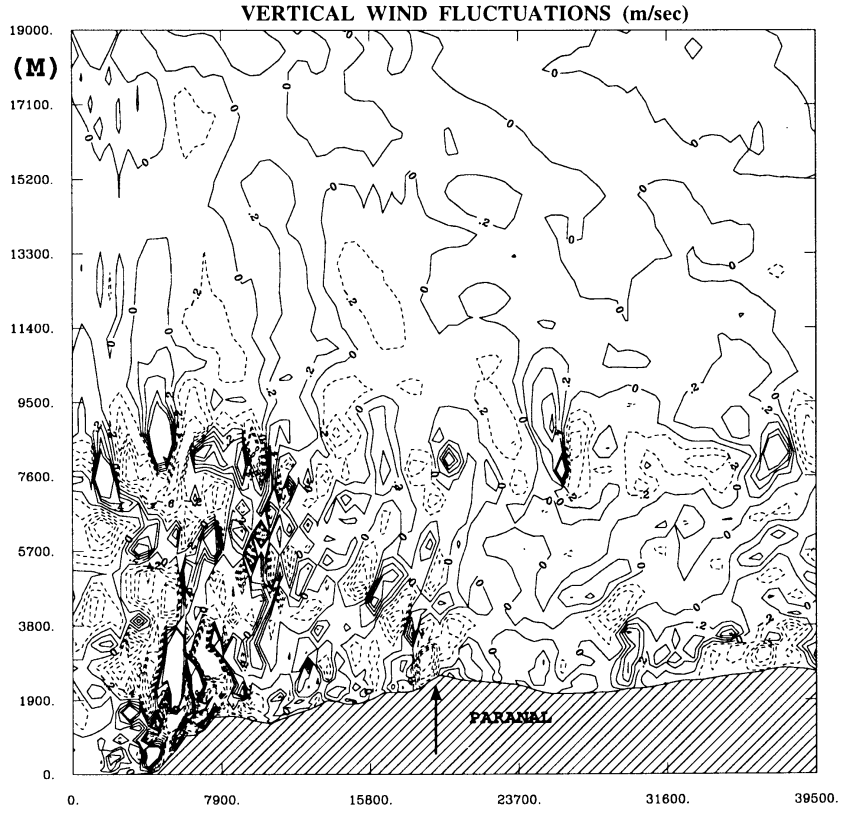

Fig. 3. Vertical wind fluctuations east-west vertical section across Paranal mountain after 4 hours simulation time during the 16/5/93 night (PARSCA93 campaign). Negative values mean a wind direction towards the ground and positive towards the top of the atmosphere

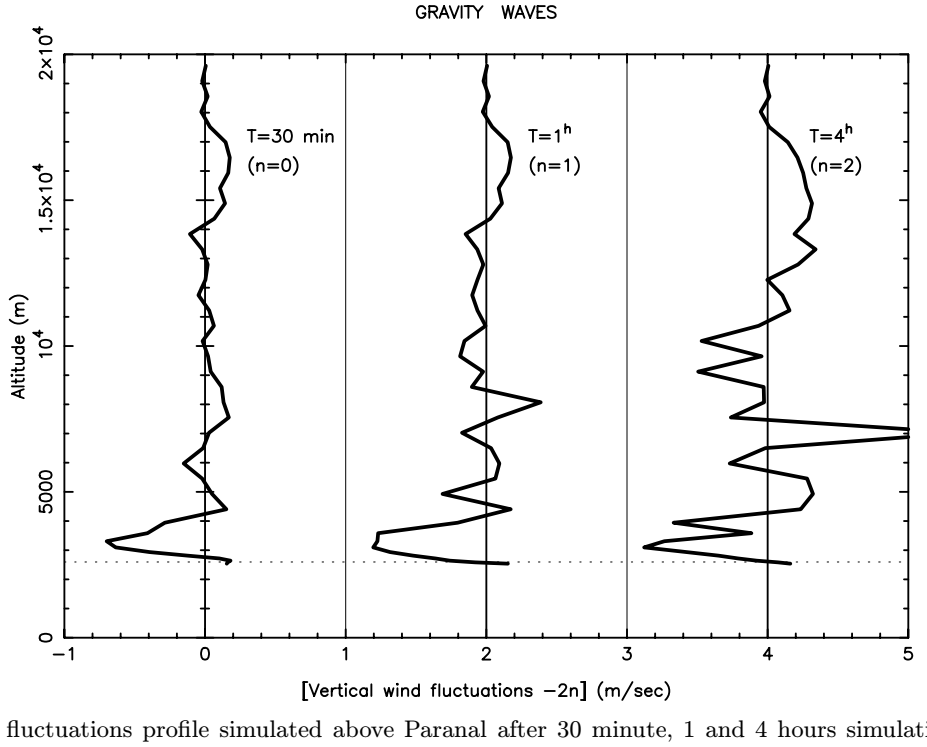

Fig. 4. Vertical wind fluctuations profile simulated above Paranal after 30 minute, 1 and 4 hours simulation time during the 16/5/93 night (PARSCA93 campaign)

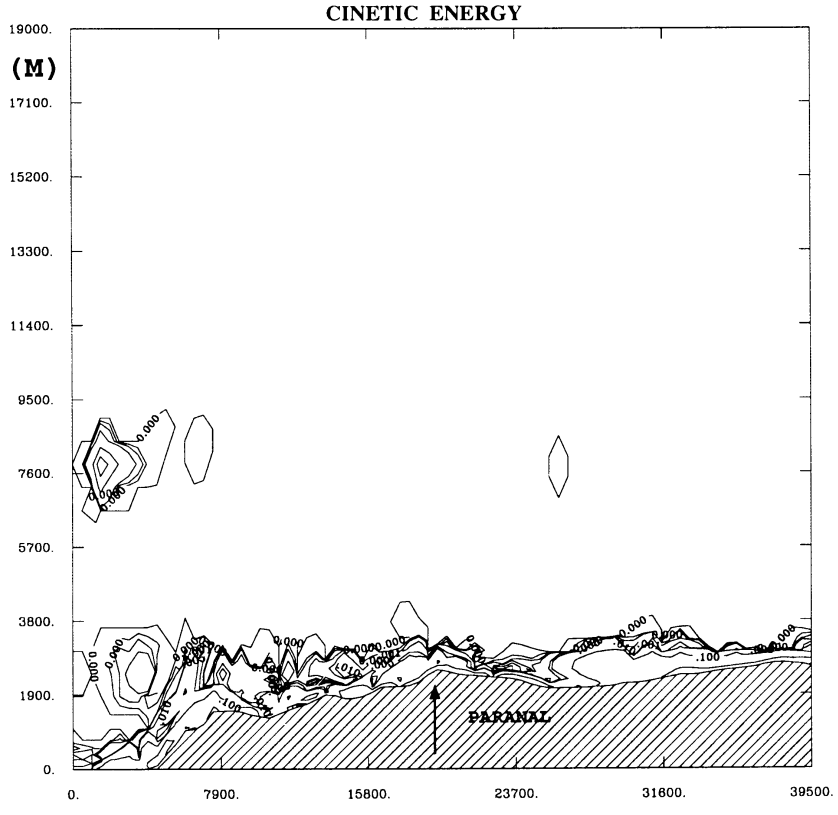

Fig. 5. Turbulent kinetic energy east-west vertical section across Paranal mountain after 4 hours simulation time during the 16/5/93 night (PARSCA93 campaign). The minimum value is 10^{-4} m/s^{-2}

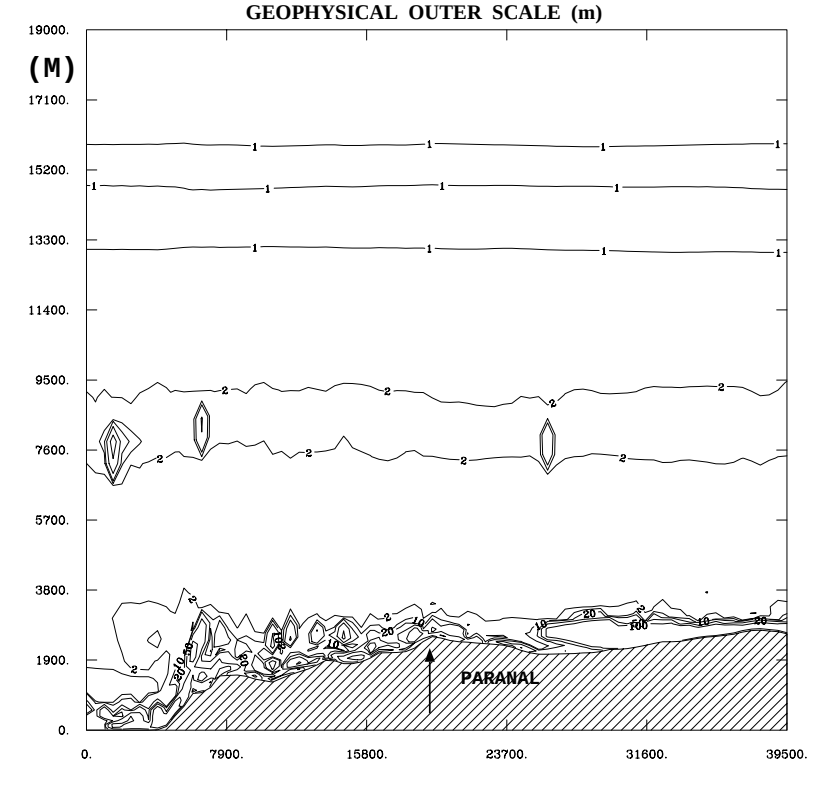

Fig. 6. As Fig. 5. Mixing length or also called geophysical outer scale

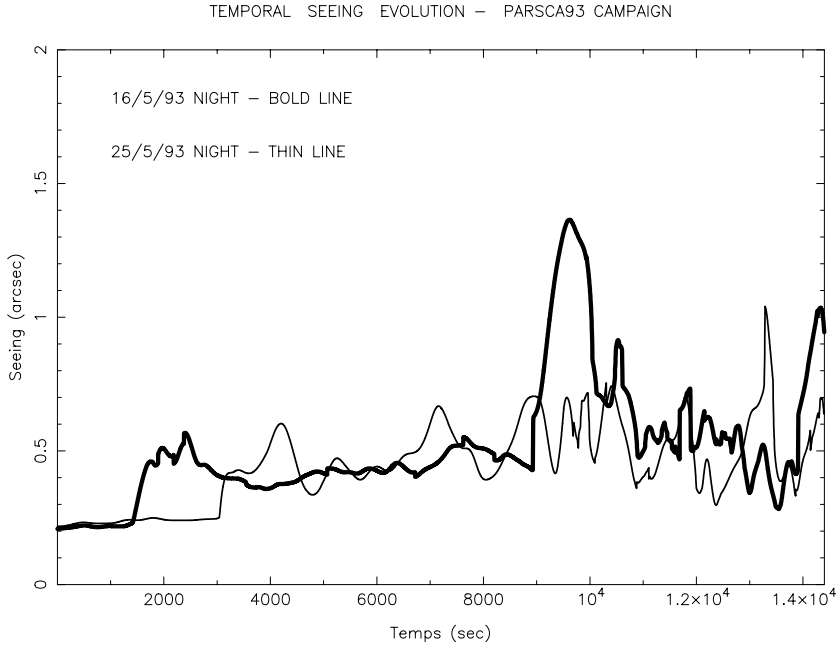

Fig. 7. Temporal seeing evolution (4 hours) during the 16/5 and the 25/5 nights (PARSCA93 campaign)

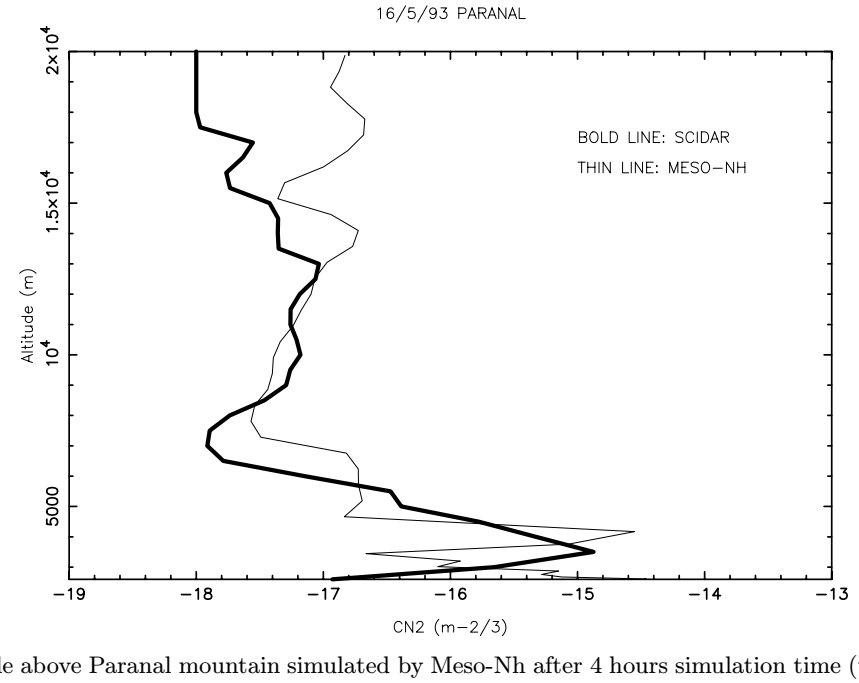

Fig. 8. C_N^2 vertical profile above Paranal mountain simulated by Meso-Nh after 4 hours simulation time (thin line) and measured by Scidar (bold line) between 01:00 and 02:00 U.T. the 16/5/93 night

shown in both potential temperature instabilities of Fig. 2 and vertical wind fluctuations Figs. 3 and 4). Moreover, in the same Fig. 8, the model reproduces the C_N^2 profile measured by Scidar during the same night but, for this case, at least 4 hours are necessary to reproduce a correct vertical profile of turbulence spatial distribution.

5.3. Sensitivity of results to horizontal resolution

A previous study (Bougeault et al. 1995) shows that the horizontal model resolution is, potentially, a critical parameter for the simulations. Two cases were studied (Bougeault 1995) using an horizontal resolution of 10 km (Lannemezan, altitude: 600 m) and 3 km (Mt. Lachens, altitude: 1700 m). In this last case, comparing the measured and simulated seeing at different grid points, the best spatial correlation was found at about 9 km

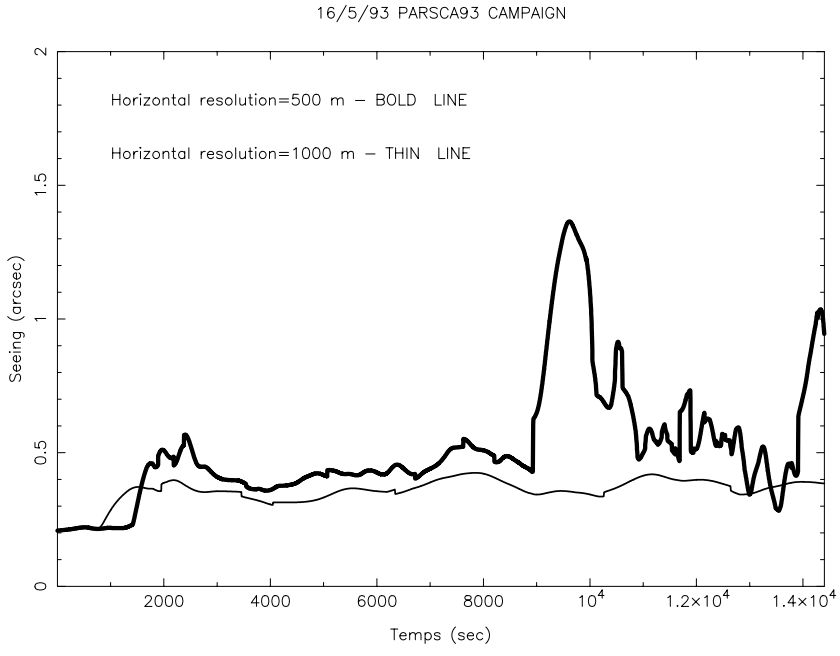

Fig. 9. Temporal seeing evolution during the 16/5/93 night simulated by Meso-Nh using two different horizontal resolutions: 1000 m × 1000 m (thin line) and 500 m × 500 m (bold line)

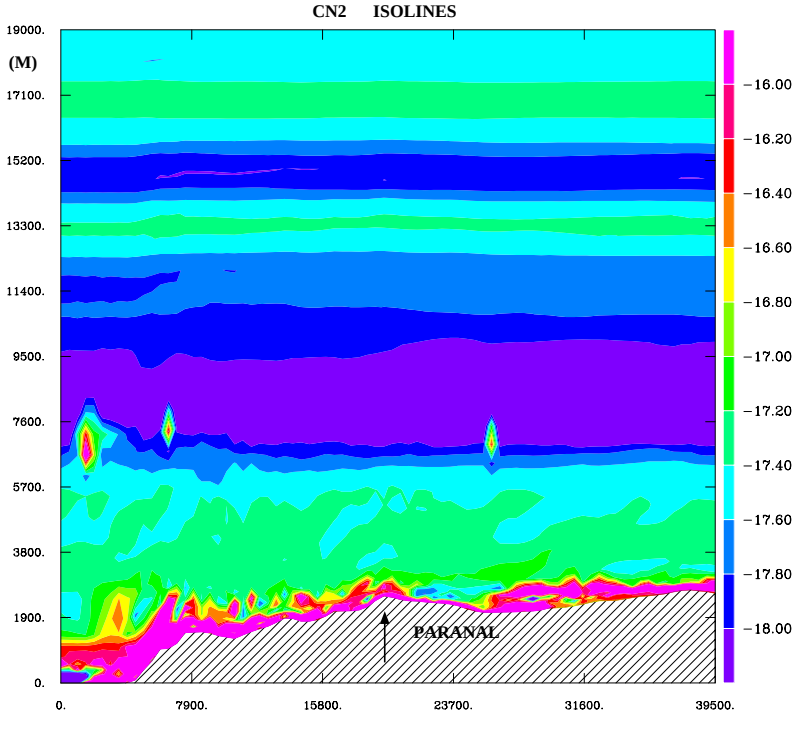

Fig. 10. 16/5/93 night (PARSCA93 campaign). C_N^2 east-west vertical section across Paranal selected over the same surface as Fig. 2. *Colour figure on Web A&AS site*

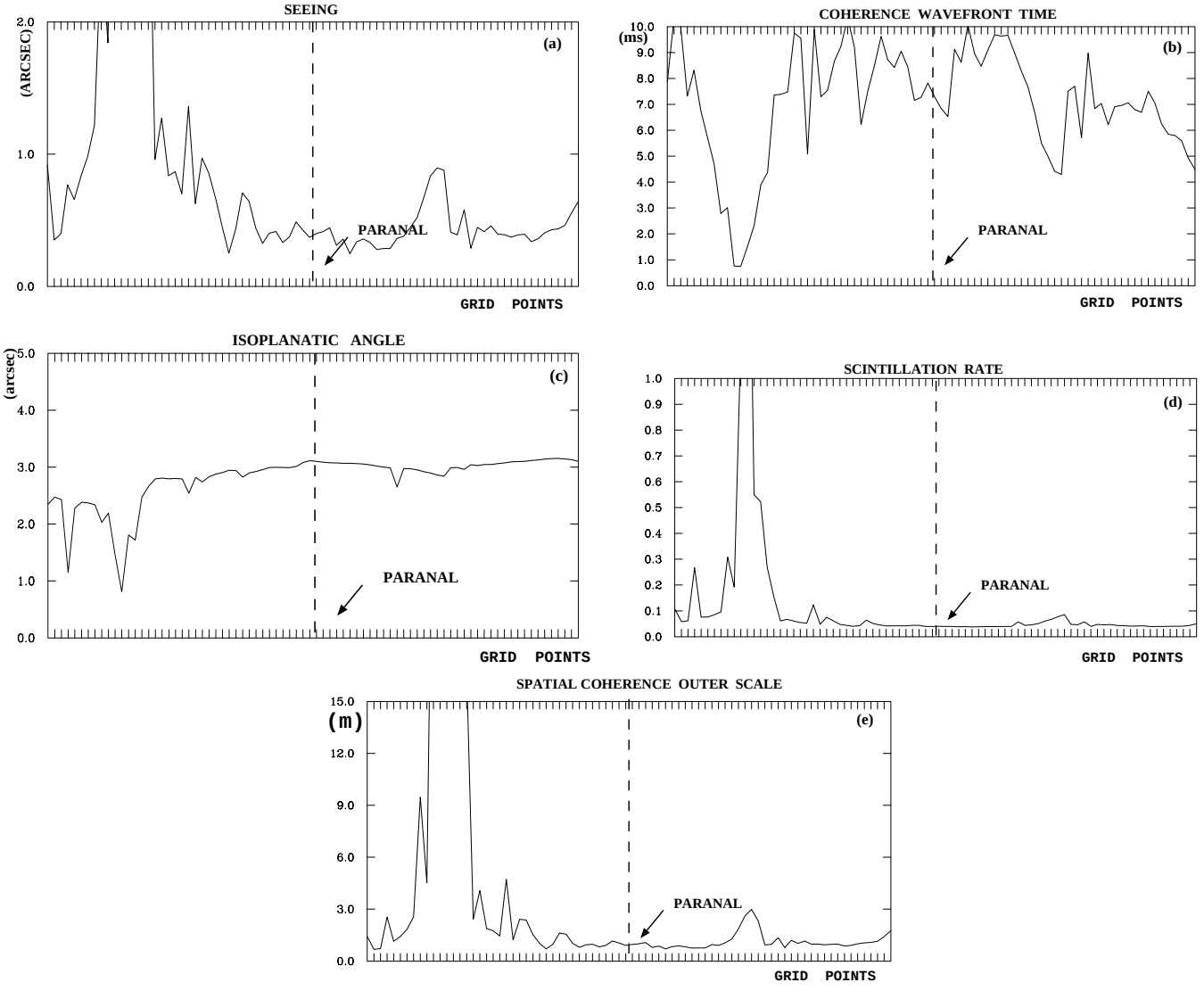

Fig. 11. As Fig. 10. East-west vertical sections of the integrated astronomic parameters coded in Meso-Nh model. **a)** Seeing ε. **b)** Coherence wavefront time $\tau_{\rm AO}$. **c)** Isoplanatic angle $\theta_{\rm AO}$. **d)** Scintillation rate $\sigma_{\rm I}^2$. **e)** Spatial coherence outer scale $\mathcal{L}_0$. Paranal is located in the center of the vertical coupe. The chilean coast is placed at the 12-th grid point

beside the mountain peak. In the conclusion the authors ascribed the low spatial correlation to the poor horizontal resolution.

Using our model, having an horizontal resolution of 500 m, we can expect to obtain more precise results, resolving the development of the turbulence generated by dynamic instabilities, that is by gravity waves. To study the impact that the horizontal resolution could have on the simulations we used different resolutions on the same geographic surface. Sampling the ground surface on grid meshes of different dimensions, we could change the model resolution and we created further orographic maps having a lower resolution. The larger the grid dimension, the greater the average action of the model and the filtered energy. Figure 9 shows, as an example, the temporal seeing evolution over 4 hour simulation time for the 16/5/93 night of the PARSCA93 campaign obtained using horizontal resolutions of 1000 m and of 500 m. With the higher resolution configuration, the seeing fluctuations related to the $C_{\rm N}^2$ layers produced during the night at different altitudes are enhanced. This shows that the horizontal grid model dimension is a critical parameter for an operational model.

5.4. Model output relevant to astronomy

In the following, typical model outputs related to the same 16/5/93 night of the PARSCA93 campaign show how the simulation results could be useful for flexible scheduling and site testing.

In Fig. 10 is reported an east-west $C_{\rm N}^2(x,\, z)$ vertical section centered on the Paranal and extending over 80

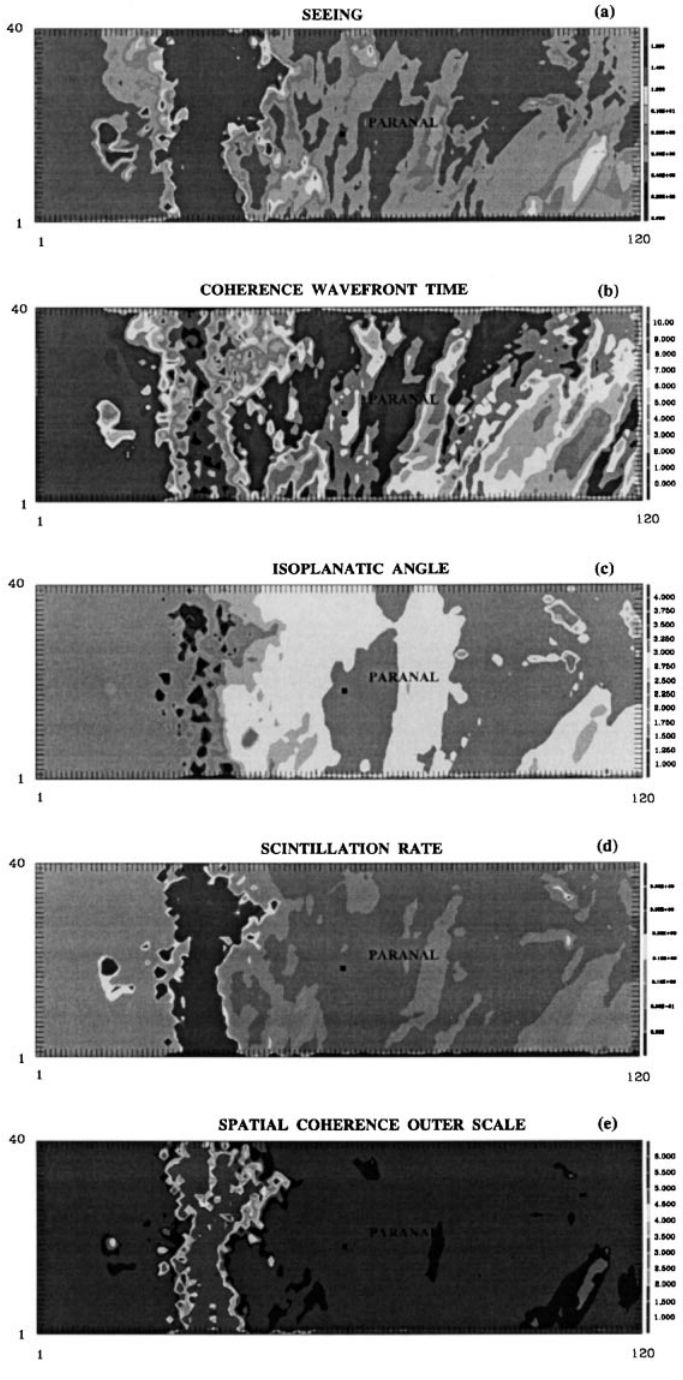

Fig. 12. Horizontal maps of the parameters showed in Fig. 11 simulated on the same surface as selected by the dashed lines in Fig. 1. **a)** Seeing ε. Color code: values between $[0-1.6]$ arcsec are represented with a step of 0.2 arcsec. Red regions are related to a bad seeing, blu regions to a good seeing. **b)** Coherence wavefront time $\tau_{\rm AO}$. Color code: values between $[0-10]$ msec are represented with a step of 1 msec. Red regions are related to a great $\tau_{\rm AO}$, blue regions to a low $\tau_{\rm AO}$. **c)** Isoplanatic angle $\theta_{\rm AO}$. Color code: values between $[1-4]$ arcsec are represented with a step of 0.25 arcsec. Red regions are related to a great $\theta_{\rm AO}$, blue regions to a low $\theta_{\rm AO}$. **d)** Scintillation rate $\sigma_{\rm I}^2$. Color code: values between $[0-50]\%$ are represented with a step of 10%. Red regions are related to a strong scintillation, blue regions to a low scintillation. **e**) Spatial coherence outer scale $\mathcal{L}_0$. Color code: values between $[1-10]$ m are represented with a step of 1 m. Red regions are related to a great $\mathcal{L}_0$, blue regions to a small $\mathcal{L}_0$. *Colour figure on Web A&AS site*

grid points (40 km). In Figs. 11a-e are reported east-west vertical sections, selected over the same 40 km, of different integrated parameters such as the seeing ε(Fig. 11a), the coherence wavefront time $\tau_{\rm AO}$ (Fig. 11b), the isoplanatic angle $\theta_{\rm AO}$(Fig. 11c), the scintillation rate $\sigma_{\rm I}^2$ (Fig. 11d) and the spatial coherence outer scale $\mathcal{L}_0$(Fig. 11e). In Figs. 12a-e are displayed horizontal maps of the same parameters over the geographic surface displayed in (Fig. 1). One can observe the general coherence of these model outputs. Above the chilean coast, on the west, we find large seeing values as seen in Fig. 11a and Fig. 12a. This is caused by the presence of the steep slope of this mountainous region producing the maximum rate of turbulence. Weak seeing values characterize the central region around Paranal and, finally, a more important seeing is found above higher mountains (> 3000 m) east of Paranal.

In Fig. 11b and Fig. 12b one can remark, over the coast, the minimum value for the coherence wavefront time $\tau_{\rm AO}$. What is the reason of such a different behavior of $\tau_{\rm AO}$ over the coast and over the Paranal? This parameter, defined in Eq. (27), depends on the 5/3 power of the wind intensity and on a linear power of the $C_{\rm N}^2$. Which of these two parameters has the greatest impact on the $\tau_{\rm AO}$? The turbulence above the coast is stronger than that above the Paranal (Fig. 10). The altitudes characterized by the strongest wind (jet-stream) are typically 12 km and, at this fixed altitude z, the wind intensity can reach 60 m/s but it is quite constant over the *x, y* direction. The wind intensity in the low atmosphere blows at a slower intensity $[1-10]$ m/s but it is generally more variable in the *x, y* direction. In order to better discriminate the different contributions provided by the turbulence ($C_{\rm N}^2$ profiles) and the velocity $v_{\rm AO}$ in the $\tau_{\rm AO}$ estimation Eq. (27) we computed (Table 1) the r_0, $v_{\rm AO}$ and $\tau_{\rm AO}$ over the whole atmosphere $[0-20]$ km, the first $[0-4]$ km and the remaining $[4-20]$ km above the Paranal mountain (40-th grid point in Fig. 11b) and the coast (11-th grid point). Analyzing the results obtained over the whole atmosphere one can observe that the ratio $r_{0,\rm P}/r_{0,\rm C}$ is ~ 25 and $v_{\rm AO,P}/v_{\rm AO,C}$ is ~ 2. One can deduce that, in this case, the extremely little value of r_0 is the principal cause of the strong decrease of $\tau_{\rm AO}$ above the coast. Moreover, we can affirm that such a little value of r_0 is ascribed to near ground turbulence. In fact, we find over $[0-4]$ km the same $r_0 = 1.33$ cm computed over the whole atmosphere. $\tau_{\rm AO}$ becomes sensitive to the fluctuations of the velocity $v_{\rm AO}$ when we analyze only the free atmosphere turbulence $[4-20]$ km contributions. In this part of the atmosphere the ratio $r_{0,\rm C}/r_{0,\rm P}$ is ~ 1.14 and $v_{\rm AO,P}/v_{\rm AO,C}$ is ~ 1.49, that is, in this case, the contributions provided by the $v_{\rm AO}$ variation is greater than the r_0 one and, ignoring the first 4 kilometers, $\tau_{\rm AO,C} > \tau_{\rm AO,P}$.

As the coherence wavefront time, the isoplanatic angle (Fig. 11c, Fig. 12c) decreases over the coast. It maintains a more or less constant value over the interior region. One can observe that, in this case, the principal cause of a decreasing value of $\theta_{\rm AO}$, from 0.3 to 0.1 arcsec, is the near ground turbulence present above the coast.

The scintillation profile is strongly correlated to the seeing one (Fig. 11a, Fig. 11c). A uniform value is observed on the broad central region except for two little peaks at about 10 km to the east and west of Paranal. In Fig. 12c) one can remark a non realistic value ($\sigma_{\rm I}^2 > 1$) of the scintillation rate above the chilean coast. This is due to the fact that Eq. (24) is obtained with the weak perturbation theory (Tatarski 1995), which is not verified in this area. It is known that the scintillation rate is proportional to the $C_{\rm N}^2 \cdot \delta h$ turbulence intensity only in the range $\sigma_{\rm I}^2 < 0.3$. For a greater $C_{\rm N}^2\ \delta h$ values the $\sigma_{\rm I}^2$ reaches a saturated value of about 1. This means that any $\sigma_{\rm I}^2$ value greater of this threshold is not significant. Finally, one can observe in Fig. 11e and Fig. 12e that the outer scale $\mathcal{L}_0$increases above the region of maximum $C_{\rm N}^2$ production, that is over the coast, and at about 10 km at the east of the Paranal. One notes that the spatial outer scale reaches very low values over the Paranal area (< 1 m). In spite of the still open discussion in the astronomic community about the $\mathcal{L}_0$estimation, these values agree with those found by some authors (Nightingale et al. 1991; Fuchs 1995) and they are supported by the physical mechanism recently proposed (Coulman et al. 1995) to explain the optical turbulence formation.

In the introduction of this paper we remembered that all the parameters affected by the optical turbulence have a stochastic behavior. During a night, thin turbulent layers can appear and disappear at different altitudes and times. Most simulation results presented here are sampled at an interval time of the order of 30 minutes or 1 hour. In order to fill this lack of information in the temporal scale we modified the code to have a further output. It is now possible to follow the temporal evolution of the $C_{\rm N}^2$ profiles simulated at a precise point (x_0, y_0) with a sampling time of about 2 minute. In Fig. 13 is reported an example of such a temporal $C_{\rm N}^2(h,\, t)$ output obtained over Roque de los Muchachos site in Canaries Isles. One can remark the presence of a strong turbulent layer at ground level, persisting during the whole night and a more variable turbulent structure at about 10 km. It is interesting to note that, during the first 30 minutes, the model has not yet reached an orographic adaptation. This tool could make simpler a comparison with Scidar measurements and it could be helpful to better define the forecast time.

6. Forecasting with a numeric model

Is it possible to make a real forecast with our model? To answer this question it is mandatory to define what *"forecast"* means.

In a forecast process three different concepts of time have to be considered: an adaptation time of the model to the orography $t_{\rm A}$, a prevision time t_P and a time of the production of prevision $t_{\rm PP}$.

Table 1. v_{AO} and r_0 contributions to the coherence wavefront time τ_{AO} over Paranal (40-th grid point in Fig. 11b) and the coast (11-teen grid point in Fig. 11b). In the first two lines are reported the values of τ_{AO}, v_{AO} and r_0 computed over the whole atmosphere $[0-20]$ km. In the next lines are reported the same parameters computed on the near ground atmosphere $[0-4]$ km and the free atmosphere $[4-20]$ km

	PARAMETERS	τ_{AO} (msec)	v_{AO} (m/s)	r_0 (cm)
$[0-20]$ km	PARANAL	7.75	15.03	37
	COAST	0.57	7.16	1.33
$[0-4]$ km	PARANAL	11.79	8.17	31
	COAST	0.58	7.13	1.33
$[4-20]$ km	PARANAL	12.23	18.30	72
	COAST	20.62	12.27	82

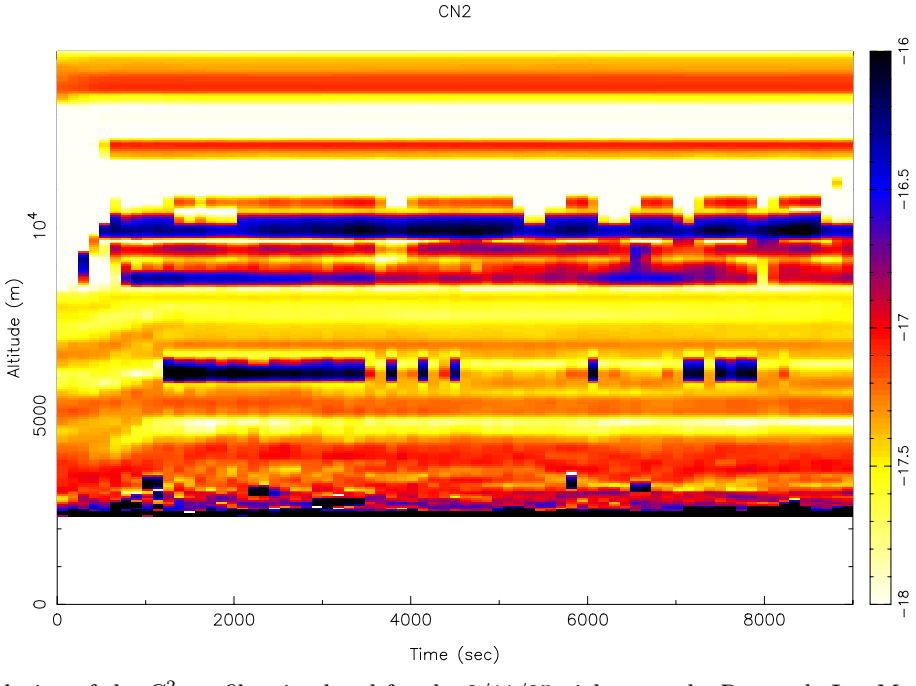

Fig. 13. Temporal evolution of the C_N^2 profiles simulated for the 3/11/95 night over the Roque de Los Muchachos Observatory in Canaries Isles. *Colour figure on Web A&AS site*

t_A is the time that the model needs to reach a thermodynamic and kinetic equilibrium already discussed in Sect. 5.2. Generally, it will depend on the geographical characteristics and from the initialization method. If the model is initialized with an unperturbed flow (this is the case for our simulations), the adaptation time is longer than that obtained with a flow in a quasi-equilibrium state. This last initialization mode consists on taking, over the domain surface, the (P, T, $\boldsymbol{V}$) fields adapted to the orography at a synoptic scales, that is at scales greater than the horizontal resolution used. The prevision time t_P is the time at which the model forecasts the atmospherical parameters. The t_{PP} time is a *"lost technical time"* for a customer. It represents the time necessary to provide a forecast depending on many different elements such as the computer memory capacity, the computation speed, the gestion of the computer memory. We think that t_{PP} will still decrease in our case in the near future, because the replacement of the conventional vector-processing computer Cray with a parallel processor that will allow simultaneous calculations for many grid points at an higher speed. The value of a forecast degrades rapidly as t_{PP} approaches t_P. Clearly the t_{PP}/t_P ratio must be less than one and t_{PP} must be optimized for each kind of forecast (24, 18, 12 and 6 hours). Hence t_{PP} does not constitute a limitation parameter even for the shortest forecasting (6 hours).

In this paper we limit our analysis to the t_A time. We showed in the previous paragraph (Fig. 7 and Fig. 9) that t_A, using such a geographic domain and initialization method, is as long as at least 30 minutes. Moreover, one can observe that in these simulations, the important turbulent layer near the ground is generated by the model only after $3-4$ hours. We can hope to decrease this

Table 2. Summary table of the zenith angle $\cos(\gamma)$ and chromatic λ dependence of the optical turbulence parameters coded in the model

Parameter	Zenith angle	Wavelenght
ε	$(\cos\,\gamma)^{-3/5}$	$\lambda^{-1/5}$
$\tau_{\rm AO}$	$(\cos\,\gamma)^{3/5}$	$\lambda^{6/5}$
$\theta_{\rm AO}$	$(\cos\,\gamma)^{8/5}$	$\lambda^{6/5}$
$\sigma_{\rm I}^2$	$(\cos\,\gamma)^{-11/6}$	$\lambda^{-7/6}$
$\mathcal{L}_0$	//	//

time by optimizing the initialization procedure. Knowing (Racine 1996; Munoz-Tuñón et al. 1997; Sarazin 1997) that the seeing characteristic time (decorrelation time) for good sites is of the order of $20-30$ minute, we could take a minimum value of $t_{\rm A}$ of the same order of magnitude.

The results that we show in this paper check the model ability to reproduce a 3D atmospheric turbulence distribution but we cannot give a precise temporal location to our simulations, that is we did not yet provide a real *"forecasting"*. Only using the forecasting products of a meteorologic center such as the ECMWF we can estimate the real forecasting performances of this technique and give an estimation of $t_{\rm P}$. In the ECMWF/WCRP Level III-A Global Atmospheric Data Archive for example, the data are classed in different sets; we should be able to provide 6-hour forecast values from the ECMWF/TOGA Supplementary Fields Data Set and 24-hour forecast values from the Extension Data Set.

7. Perspectives and conclusions

What are the possible future implementations for this technique?

In order to refine the performances of the model some modifications could be suggested. Introducing a zenithal ($\cos\gamma$) and chromatic (λ) dependence in the code, one could forecast, at a precise t_0, for a fixed telescope position (x_0, y_0), the values of all the parameters coded in the model for each line of sight and for each spectral band. In Table 2 are reported the zenith angle and the chromatic dependence of the optical turbulence parameters coded in the model. The possibility to reconstruct 3D maps of the optical turbulence could be an efficient tool for site testing. The numerical technique could substitute or complete the data provided from the often expensive campaigns organized to build a climatologic data base of a particular site. The model could give a complete 3D description over an extended surface at the same time for different sites using the same tool.

In the context of flexible scheduling this technique could give a contribution in the gestion of the observing modes at a telescope. Particularly favorable conditions could be used for High Angular Resolution techniques as the Interferometric one and a more modest seeing could justify a Direct Imaging or a Spectroscopy technique. Moreover, in order to determine the accuracy of the wavefront sensor and the performances of the adaptive telescope we could forecast 2D maps of the rms residual wavefront error $\Delta\phi$ obtained over an aperture D for an adaptive optics system achieving perfect tilt compensation (Fried 1965) and the Strehl ratio for this perfect tilt removal (Chester et al. 1990). The model could be an useful tool, not only for the gestion of the observing mode but also for the gestion of the focal instruments placed at the focus of the telescope.

A three-dimensional picture of the turbulence provided by Meso-Nh could be used as a more realistic model than the empirical Hufnagel model (Roddier 1981) or the simpler *single layer* model frequently employed.

Thus knowing the altitude of each layer as an output of our model, it becomes possible to help to implement MCAO (Multiconjugate Adaptive Optics) technique (Tallon 1992).

In this paper we describe the general characteristics of the Meso-Nh model, the parameters coded in the model characterizing the optical turbulence and the applications that this tool could have for site testing, for optimization of the adaptive optics technique and for flexible scheduling. We showed both the potentiality of this technique and the general coherence of the informations that it could provide. We proved the model sensitivity to the orographic effects and we tested the influence of the horizontal resolution on the simulations outputs. The model ability to reproduce a correct spatial distribution of the optical turbulence is supported by a comparison between Scidar measurements and Meso-Nh simulations (Fig. 8).

The challenge for a future implementation of this technique in the astronomy field depends from:

- the sensitivity and the accuracy of the method;
- the statistical reliability of the model compared to other techniques already tested for flexible scheduling, as the forecast for persistence;
- the model performances using the prevision products provided by the meteorological centers.

In the following article, we give the results of a systematic statistic analysis taken over 15 nights of the PARSCA93 (Fuchs et al. 1994) campaign (5/1993). Useful informations about the sensitivity and the statistic reliability are provided in this paper.

Acknowledgements. This work is supported by contract (Technical Report UNI-17400-0004) from ESO. The authors are grateful to M. Sarazin for his constant and dedicated presence in this feasibility study. They wish to thank the GMME team of the Centre National de Recherche Meteorologique for their scientific collaboration and logistical help. In particular, they gratefully acknowledge the many helpful discussions with J. Stein, P. Jabouille, J.L. Redelsperger and J.P. Lafore. The authors thank C. Coulman for his helpful comments and revision of the draft.

References

Andre J.C., et al., 1978, J. Atmosph. Sci. 35, 1861
Aussem A., et al., 1994, Vistas Astron. 38, 357
Beckers J.M., 1993, Ann. Rev. Astron. Astrophys. 31, 13
Bely P., 1983, ESO Workshop-La Silla, 4-6 October 13, 55
Borgnino J., 1990, Appl. Opt. 13, 1863
Bougeault P., Lacarrere P., 1989, Monthly Weather Rev. 117, 1872
Bougeault P., et al., 1995, Appl. Opt. 34, 3481
Chester S., Gardner, et al., 1990, Proc. of the IEEE 78, 1721
Couleman C., Gillingham P.R., 1986, PASP 98, 376
Coulman C., et al., 1988, Appl. Opt. 27, 155
Couleman C., et al., 1995, Appl. Opt. 34, 5461
Cuxart J., et al., 1995, 11th Symp. Boundary Layers & Turb. 13, 409
Di Serego Alighieri S., 1996, ASP Conf. Series-New Observing Modes for the Next Century 87
Di Serego Alighieri S., 1997, 3G Conf.-Padova, 7 January 1997 97
Fried D.L., 1965, PASP 55, 1427
Fried D.L., 1979, Optica Acta 26, 597
Fuchs A., Vernin J., 1994, VLT Technical Report VLT-TRE-UNI-17400-0001
Fuchs A., 1995, PhD Thesis-Universite de Nice, France
Lafore J.P., et al., 1998, Ann. Geophys. 16, 90
Martin F., et al., 1994, A&A 282, 1021
Masciadri E., et al., 1997, Final Report - VLT - Technical Report UNI-17400-0004, 97
Meteorological Monographs, 1990 Blumen (ed.) Atmospheric processes over complex terrain
Muñoz-Tuñón C., et al., 1997, A&AS 125, 183
Murtagh F., Sarazin M., 1983, PASP 105, 932
Nightingale N.S., Buscher D.F., 1991, MNRAS 251, 155
Racine R., 1996, PASP 108, 372
Redelsperger J.L., Sommeria G., 1981, Boundary Layer Met. 21, 509
Roddier F., 1981, Progress Opt. Vol. XIX, No. 18, 283
Roddier F., et al., 1982, J. Opt. Paris 13, 63
Roddier F., et al., 1982, J. Opt. Paris, 13, 263
Sarazin M., Roddier F., 1981, A&A 227, 294
Sarazin M., 1997, SPIE - San Diego, August 125, 3125
Sarazin M., 1997, The Messenger (October) 97, 5
Sarazin M., 1997, AO'95 - Adaptive Optics Topical Meeting - Garching, October 2-6
Tallon M., Foy R., Vernin J., ESO Conference 42 on Progress in Telescope and Instrumentation Technologies - Garching, April 27-30
Tatarski V., 1995, Wave propagation in a turbulent medium
Tennekes H., Lumley J.L., 1972, A First Course in Turbulence. The Mit Press
VanZandt T., et al., 1978, Radio Sci. 13, 819
VanZandt T., et al., 1981, 20th Conf. on Radar Meteorology. Boston 30 Nov./3 Dec., p. 129
Vernin J., Azouit M., 1983, J. Opt. Paris 14, 5
Vernin J., Azouit M., 1983, J. Opt. Paris 14, 131
VLT - Site selection working group, 1990 VLT Report 62
Wyngaard J.C., et al., 1971, J. Opt. Soc. Am. 61, 1646